



30 **1 Introduction**

31

32 Air pollution in urban areas has become a concern in our society because it represents
33 a major risk to human health and the environment (WHO, 2019). Air quality is often expressed
34 as the state of air pollution in terms of gaseous pollutants concentrations as well as size and
35 number of particulate matter that may affect human health, ecosystems and climate (Monks et
36 al., 2009). Integral understanding of air pollution requires knowledge about the sources,
37 pollutants, chemical composition and spatial distribution, and their transport phenomena in the
38 atmosphere (EEA, 2019).

39

40 Madrid, Spain, has suffered from severe air pollution in recent years, with episodes of
41 large nitrogen dioxide (NO₂) and ozone (O₃) concentrations. In an effort to control and reduce
42 high pollution events, the local government has enforced some traffic restriction measures
43 (Izquierdo et al., 2020) and has set up several in-situ air quality monitoring stations over the
44 city's metropolitan area. These in-situ instruments -as of today- cannot measure some important
45 trace gases present in the atmosphere and their values are only representative of the immediate
46 surrounding of the instruments and at surface level. There is therefore a need for mesoscale
47 analysis (both in horizontal and vertical) of urban air pollution that could complement the in-
48 situ measurements. With this aim, we have deployed Multi AXis Differential Optical
49 Absorption Spectroscopy (MAXDOAS) instruments for air pollution measurements in Madrid.
50 MAXDOAS is a widely used technique for the detection of trace gases in the atmosphere and
51 it is based on the wavelength dependent absorption of scattered sunlight by atmospheric
52 constituents (Platt and Stutz, 2008). In addition to routinely monitored, regulated species such
53 as NO₂ and O₃, MAXDOAS provides mesoscale measurements of other trace gases that are
54 relevant to understand atmospheric chemistry, such as nitrous acid (HONO), formaldehyde
55 (HCHO) or glyoxal (CHOCHO). Over the past few years, we have reported trace gas
56 measurements in Madrid using the MAXDOAS technique (Wang et al., 2016; Garcia-Nieto et
57 al., 2018; Benavent et al., 2019) as well as pollutants trend analysis and chemical transport
58 modelling (Borge et al., 2018; Cuevas et al., 2014; Saiz-Lopez et al., 2017).

59

60 For this work, a new two-dimensional MAXDOAS instrument (which will be described
61 in Sect. 3 and will be hereafter referred to as MAXDOAS-2D) has been built, tested and set up
62 to take continuous measurements in Madrid. This instrument represents a follow-up



63 development to our previous one-dimensional instrument (MAXDOAS-1D, see Wang et al.,
64 2016) that incorporates the capability of moving in the azimuthal dimension, therefore allowing
65 the collection of spectra pointing at any desired angular direction. This additional capability
66 allows the measurement of both the horizontal and vertical trace gas (e.g. NO₂) distribution
67 throughout the city and in turn the generation of two-dimensional maps of trace gas
68 composition.

69

70 Here we present two months of MAXDOAS-2D measurements of scattered sunlight
71 spectra. The measurements were taken from May 6, 2019 to July 5, 2019, with focus on the
72 evaluation of NO₂ vertical concentration profiles and the characterization of horizontal light
73 paths lengths. This represents the first two-dimensional MAXDOAS measurements in Madrid.
74 An assessment of the relation between the MAXDOAS analysis and the in-situ instruments in
75 the city was carried out. Sect. 2 provides details of the DOAS technique while Sect. 3 describes
76 the experimental setup. The inversion methods and the atmospheric parameters chosen for the
77 analysis is detailed in Sect. 4. The two-dimensional NO₂ distributions, an evaluation of the
78 light path geometries, along with their relative probabilities, and an assessment of horizontal
79 mixing ratio gradients near the surface are discussed in Sect. 5. Finally, Sect. 6 contains
80 conclusions and possible future work.

81

82 **2 Brief introduction to the DOAS method**

83

84 The absorption spectroscopy field has been developed for several decades within
85 different research disciplines (such as remote sensing, astronomy or atomic and molecular
86 physics). Its foundation relies on the absorption of radiation when interacting with a certain
87 sample. The basic idea is described by the Beer-Lambert law, which models the exponential
88 attenuation of spectral irradiance when it traverses a certain sample that contains some absorber
89 species:

90

$$91 \quad I(\lambda, L) = I_0(\lambda) \exp \left(- \sum_i \int_0^L \sigma_i(\lambda) \rho_i(\lambda) ds \right) \quad (1)$$

92

93 where λ is the radiation wavelength, σ_i and ρ_i stand for -respectively- the absorption
94 cross section and concentration of a given absorber i along the path, while the pair I_0 and I



95 represent the spectral irradiances at the beginning and end of the process at study. The
96 absorption processes are integrated over the photon paths (with infinitesimal path ds) and
97 summed over every present absorber (Platt and Stutz, 2008).

98

99 Specifically, the MAXDOAS technique is based on the study of the differential spectral
100 absorption structures that are produced in the measured scattered sunlight spectra (Plane and
101 Saiz-Lopez, 2006; Platt and Stutz, 2008). The main principle is based on identifying the
102 narrowband absorption features within the measured optical density taking out the broadband
103 optical density, mainly generated by Rayleigh and Mie scattering, as well as by instrumental
104 effects. On the other hand, an analogous process is done on the trace gases absorption cross
105 sections by means of filtering out the broadband spectral features, hence producing the so-
106 called differential absorption cross sections, which are unique for each trace gas, acting as their
107 “fingerprints” and therefore enabling their specific detection.

108

109 For MAXDOAS, I_0 stands for the solar spectrum (known as the Fraunhofer spectrum,
110 with no Earth atmospheric absorptions), while I represents the recorded ground-based
111 spectrum, which includes all the absorption and scattering processes. However, and since the
112 actual photon path is difficult to determine with accuracy (see Sect. 4), the MAXDOAS
113 calculations are done using relative absorptions between two different optical paths: a zenith
114 spectrum -that contains less absorptions and is assumed as a reference spectrum- and other
115 spectrum pointing to a given elevation angle. Therefore, the direct product of the method is the
116 Differential Slant Column Density (DSCD), which can be defined as the difference in the
117 integrated concentration of a given absorber between the two selected pointing directions (more
118 details about the numerical procedure that lies behind can be found in Honninger et al., 2004,
119 Plane and Saiz-Lopez, 2006 and Platt and Stutz, 2008). Finally, these DSCDs are used as the
120 main input for the profile retrieval algorithms, which try to reconstruct the photon paths that
121 result in the measured DSCDs. This final step produces the vertical concentration profiles
122 (Sect. 4).

123 **3 Experimental**

124

125 Briefly, MAXDOAS-1D instruments consist of a light collector attached to a stepper
126 motor that scans the atmosphere at different Viewing Elevation Angles (VEA, see Fig. 1). The
127 main feature added to the MAXDOAS-2D instrument is an additional stepper motor for the



128 azimuthal movement, hence allowing the light collector to freely point to any angular direction
129 in the atmosphere. This allows the evaluation of trace gases absorptions for different Viewing
130 Azimuth Angles (VAAs) (Fig. 1).

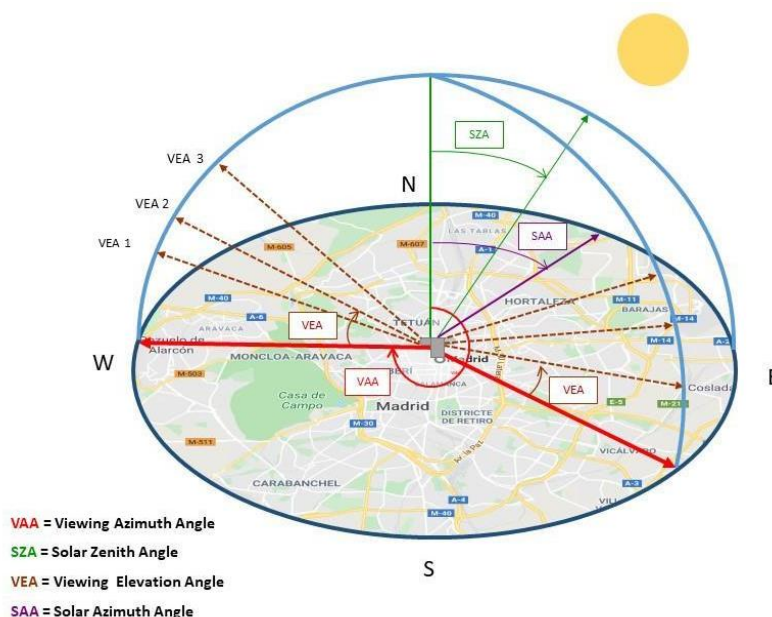
131

132 **3.1 MAXDOAS-2D description**

133

134 A new MAXDOAS-2D instrument (Fig. 2) was built by the Atmospheric Chemistry
135 and Climate group at the Institute of Physical Chemistry Rocasolano (IQFR, CSIC). Its main
136 elements are based on our previous MAXDOAS-1D instrument: a light collector attached to a
137 stepper motor, along with a focusing lens (80 mm focal length) are responsible for collecting
138 the scattered sunlight. An Ocean Optics, SMA 905 optical fiber of 1-meter length conducts the
139 light through an Ocean Optics, HR4000 spectrometer (which incorporates a linear silicon CCD
140 array as detector). The spectrometer wavelength ranges roughly from 300 nm to 500 nm and
141 offers an estimated spectral resolution (full width at half maximum) of about 0.5 nm. As
142 explained before, an additional stepper motor was included to make the azimuthal movement
143 possible. The instrument incorporates all its components in an outdoor unit. Therefore, to
144 maintain the spectrometer temperature as steady as possible -for both mechanical and
145 wavelength calibration purposes- a Peltier cell was included. Additionally, an UPS device
146 provides the power supply and eliminates possible strong power peaks. Two webcams take
147 pictures of the cloud cover at each VAA, and monitor the instrument itself. The instrument is
148 quite autonomous and it runs on a homemade Java software. This software controls the
149 movement, the spectra collection and recording, the surrounding accessories and automatically
150 keeps it continuously measuring as long as the Sun is over the horizon.

151



152

153 **Figure 1.** MAXDOAS-2D geometry diagram, the background of this picture represents the
154 Madrid city center taken by © Google Maps.

155

156 3.2 Location

157

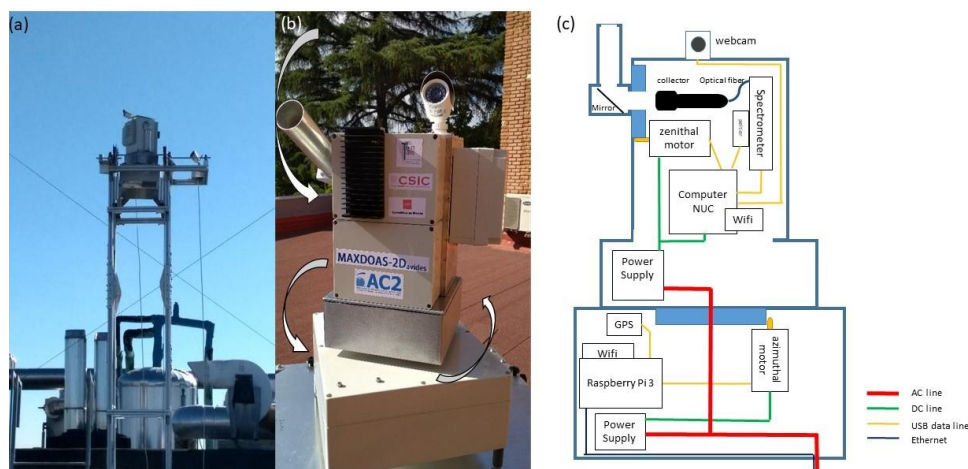
158 The MAXDOAS-2D instrument is located at the main campus of the Spanish National
159 Research Council (CSIC) in Madrid (Spain). It is placed on the roof of the Instituto de Ciencias
160 Agrarias (ICA) at a latitude of 40.4419° N and a longitude of 3.6875° W. The height of the
161 building is approximately 70 m above ground level. This location in downtown Madrid can be
162 classified as an urban site, with the usual weather of continental areas at mid-latitudes (i.e. hot
163 and dry summers and cold winters), with prevalence of clear sky days during the year.

164

165 Due to some obstacles that blocked a clear view in some of the VAAs, a small
166 aluminum tower was built to overcome the viewing obstacles and the MAXDOAS-2D
167 instrument was fixed on top of it (see Fig. 2). Once the instrument was set up, we aligned it for
168 both angular movements -azimuthal and zenithal- with respect to the geographical north and
169 the local horizontal (i.e. perpendicular to the gravitational plumb), respectively. This process
170 was performed in two steps: first, the light collector was coarsely oriented using levels and a
171 compass. Then, the alignment was refined doing a vertical scan of the Sun (which has a very



172 well-known position vector) and its angular surroundings at several different times of a clear
173 sky day. The angular differences between the measurements and the center of intensity of the
174 registered spectra (a similar approach was done in Ortega et al., 2015) were estimated and the
175 associated correction applied to the instrument.
176



177
178 **Figure 2.** a) aluminum tower with the instrument installed on top of it; b) MAXDOAS-2D
179 instrument; c) MAXDOAS-2D scheme.

180

181 3.3 Measurements set up

182

183 In order to sample and analyze a representative portion of the atmosphere over Madrid,
184 selected angular directions were chosen. Starting at a VAA of 0° (pointing to the north), the
185 MAXDOAS-2D rotated clockwise using steps of 20° in azimuth. In each azimuth direction, the
186 ensuing VEA vector was used: 1, 2, 3, 5, 10, 30 and 90 degrees. Therefore, an entire azimuthal
187 lap was completed when the light collector was back again at VAA of 0 degrees.

188

189 For every measured spectrum, the spectrometer was able to correct for both electronic
190 offset and dark current effects. Other important parameters for the measurements such as the
191 integration time and the number of scans taken in each angular direction were automatically
192 calculated by the software. More specifically, for this study we set the goal of completing an
193 azimuthal lap in approximately one hour (mainly for an easier interpretation of the results and
194 for the subsequent comparison with in-situ instruments of Madrid's air quality monitoring



195 network). Hence, we chose 24 seconds as the maximum exposure time in each angular
196 combination.

197

198 **4 Analysis methods**

199

200 Using the DOAS technique, the absorptions of the molecular oxygen dimer (O_4) and
201 NO_2 were measured for the entire campaign and for two spectral windows: 352-387 nm (UV
202 region) and 438-487 nm (VIS region). The analysis settings applied for the UV and VIS regions
203 are summarized in Tables 1 and 2, respectively. These configurations follow those used in
204 Wagner et al., 2019.

205

206 **Table 1.** DOAS spectral settings for the retrieval of O_4 and NO_2 in the UV.

| Parameter | Value |
|------------------------|---|
| Fitting window | 352-387 nm |
| Wavelength calibration | Based on reference solar atlas (Chance and Kurucz, 2010) |
| Zenith reference | Scan |
| Polynomial Order | 5 |
| Intensity Offset | Order 2 |
| Shift | All spectra and the Ring cross section were allowed to shift and stretch (order 1) in wavelength. |

| Molecule | Cross section |
|----------|------------------------------------|
| O_4 | 293 K (Thalman and Volkamer, 2013) |
| NO_2 | 298 K (Vandaele et al., 1998) |
| O_3 a | 273 K (Serdyuchenko et al., 2014) |



| | |
|------------------|--|
| O ₃ b | 223 K (Serdyuchenko et al., 2014) |
| HCHO | 297 K (Meller and Moortgat, 2000) |
| HONO | 296 K (Stutz et al., 2000) |
| Ring_a | Calculated by QDOAS |
| Ring_b | Ring_a spectrum multiplied by λ^{-4} |

207

208 **Table 2.** DOAS spectral settings for the retrieval of O₄ and NO₂ in the VIS.

| Parameter | Value |
|------------------------|--|
| Fitting window | 438-487 nm |
| Wavelength calibration | Based on reference solar atlas (Chance and Kurucz, 2010) |
| Zenith reference | Scan |
| Polynomial order | 5 |
| Intensity offset | Order 2 |
| Shift | All spectra and the Ring cross sections were allowed to shift and stretch (order 1) in wavelength. |

| Molecule | Cross section |
|------------------|------------------------------------|
| O ₄ | 293 K (Thalman and Volkamer, 2013) |
| NO ₂ | 298 K (Vandaele et al., 1998) |
| O ₃ a | 273 K (Serdyuchenko et al., 2014) |
| O ₃ b | 223 K (Serdyuchenko et al., 2014) |
| H ₂ O | 296 K (Rothman et al., 2010) |
| Glyoxal | 296 K (Volkamer et al., 2005) |
| Ring a | Calculated by QDOAS |



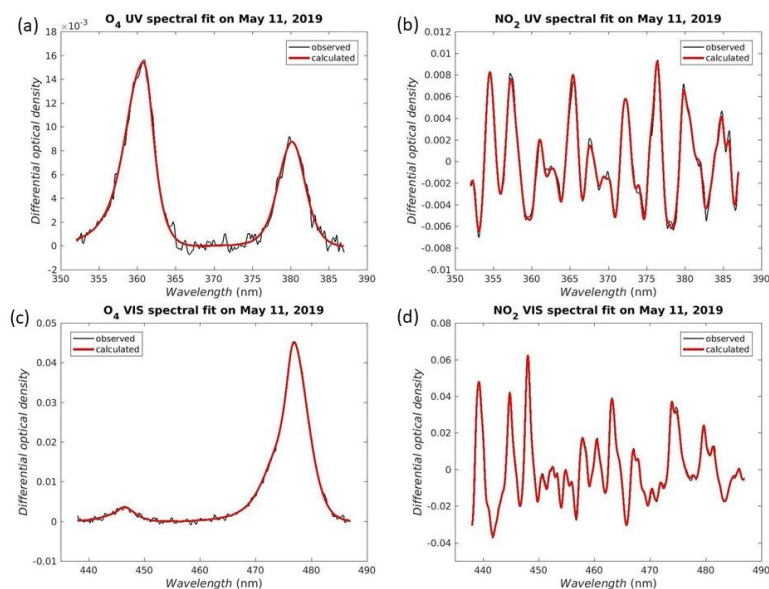
Ring b

Ring a spectrum multiplied by λ^{-4}

209

210 The selected differential absorption cross sections -along with the spectral window and
211 parameters included in Tables 1 and 2- were adjusted to the measured differential optical
212 density using the QDOAS spectral fitting software (developed at BIRA-IASB, <http://uv-vis.aeronomie.be/software/QDOAS/>). When the measured DSCD (using QDOAS) accurately
213 matches the differential optical density for a given trace gas -i.e. yielding a relatively low
214 residual- there is positive detection of that trace gas -i.e. yielding a relatively low
215 residual- there is positive detection of that trace gas. Figure 3 shows examples of spectral
216 detection of O₄ and NO₂ for both the UV and VIS regions. Once the DSCDs are obtained, they
217 are used as input for the profile retrieval algorithm, as explained in Sect. 4.2.

218



219

220 **Figure 3.** Spectral detection of O₄ (a) and (c) and NO₂ (b) and (d), red lines represent the
221 calculated optical densities and black lines are the measured optical densities.

222

223 4.1 Cloud-screening and quality filtering

224

225 The algorithms for MAXDOAS retrievals of trace gas vertical profiles are based on
226 estimating the light paths (along with their corresponding scattering probability) for a clear sky



227 day. A significant cloud cover could noticeably impact the calculations, mainly because of
228 multiple scattering effects, adding large uncertainties to the retrieval process. For this reason,
229 the set of measured spectra has to be cloud-screened, filtering out those spectra affected by
230 clouds. In order to achieve that, the cloud-free AERONET database was used. The AERONET
231 (AERosol RObotic NETwork) project is a global network of ground-based remote sensing
232 instruments established by NASA and PHOTONS
233 (https://aeronet.gsfc.nasa.gov/new_web/index.html) which measure aerosols and their optical,
234 microphysical and radiative properties. The AERONET instruments provide a long-term,
235 continuous and readily accessible public domain database of aerosol measurements worldwide.
236 These databases are reported with three quality levels, in particular, we used the Level 2.0
237 (cloud-screened and quality-assured) database provided by the AERONET instrument placed
238 in Madrid to flag the cloudy atmosphere and discard the related measured spectra. After that,
239 the remaining spectra can be regarded as cloud-free.

240

241 Since we are dealing with a non-linear, least-squares system of equations, there is a
242 notable gradient concerning the quality and uncertainties in the results. Hence, before
243 proceeding with the profiling algorithm, several quality filters were applied to the DSCDs:
244 firstly, every DSCD that yielded either a relative uncertainty larger than 1 or a residual Root
245 Mean Square (RMS) higher than 0.01 (in optical density units) was rejected. After that, we
246 estimated the DSCDs detection limit for a given trace gas as the ratio of the residual RMS (in
247 optical density units) associated to each DSCD and the maximum value of the differential cross
248 section of that trace gas. Then, we discarded the DSCDs that had an absolute value lower than
249 twice the derived detection limit (a similar approach was carried out in Peters et al., 2012).
250 Finally, we used the daily plus/minus three standard deviation criterion that AERONET applies
251 for its cloud-filtered data, keeping the DSCD that fall within plus/minus three standard
252 deviations from each daily mean.

253

254 **4.2 Inversion algorithm and vertical profiles**

255

256 We apply inversion algorithm methods to the measured DSCDs to estimate the light
257 paths and subsequently derive the trace gas vertical concentration profile. The main idea behind
258 these inversion algorithms is based on the fact that each VEA has different scattering heights
259 and light paths (Solomon et al., 1987). Therefore, a given set of measured DSCDs contains



260 information about the vertical distribution of a certain trace gas. Since higher VEAs are
261 generally related to higher scattering heights, different layers within the atmosphere can be
262 sampled, especially in the lower troposphere.

263

264 The algorithms that calculate these scattering events are called Radiative Transfer
265 Models (RTMs), and they study the transport of radiation as well as its interaction with matter.
266 There are several RTMs for atmospheric applications, but for this work we have used the
267 bePRO inversion algorithm, developed at BIRA-IASB (Clémer et al., 2010). The original
268 calculation was built based on the Optimal Estimation Method (OEM; Rodgers, 2000) and it
269 comprises two steps: first, the light paths and the vertical profiles of irradiance extinction are
270 calculated using the O₄ DSCDs; then, the target trace gas vertical concentration profile is
271 retrieved using the corresponding light paths and measured absorption. In order to do that,
272 bePRO simulates the atmospheric state characterizing several different physical phenomena
273 including pressure and temperature vertical profiles, Rayleigh and Mie scattering events (along
274 with their respective phase functions), the effect of the surface albedo, the light path geometries
275 or the irradiance extinction processes. Once the atmospheric vector state is defined, its
276 combination with a certain vertical concentration profile results in the simulated DSCDs. This
277 vertical profile is iterated until the generated set of simulated DSCDs is optimized with respect
278 to the measured DSCDs so that the residual is minimized. As a result, an optimal vertical profile
279 is obtained when the iteration is finished for each MAXDOAS cycle.

280

281 The measured O₄ DSCDs are used to estimate the light paths for each VEA since they
282 are related to the square of the atmospheric O₂ profiles, which are well-known. This profile is
283 fairly steady during the day and does not heavily depend on chemistry factors. Therefore, the
284 measured O₄ DSCDs can provide information on the irradiance extinction in the atmosphere.
285 This extinction profile, retrieved using bePRO, is usually associated with the aerosol extinction
286 coefficients and thus, its vertical integration yields the Aerosol Optical Depth (AOD). These
287 aerosol extinction profiles are required to subsequently evaluate trace gas profiles since they
288 strongly affect the relative light paths and hence the concentration profiles derived from them.

289

290 Once the light paths are computed in the previous step, an analogous process is repeated
291 for the measured DSCDs of the target trace gas, yielding the optimal vertical concentration
292 profile. The vertical integration of this concentration profile is called the Vertical Column
293 Density (VCD).



294

295 The retrieval consists of an iterative, nonlinear system of equations, and hence there is
296 no unique solution. This means that an a priori profile is needed, both for starting the iterations
297 and to avoid the final solution to be non-realistic (i.e. with no physical meaning). In order to
298 construct these a priori profiles we used exponentially decreasing curves as follows:

299

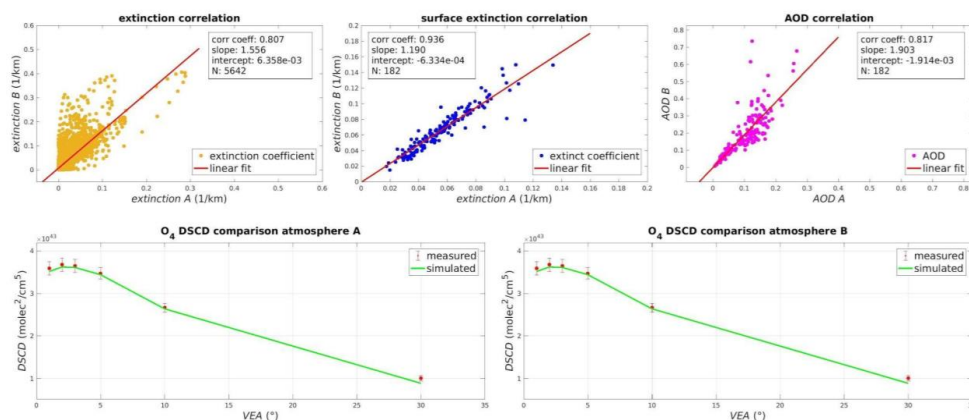
$$300 \qquad ap(z) = \frac{VC_i}{sh} \exp\left(\frac{-z}{sh}\right) \qquad (2)$$

301

302 where $ap(z)$ is the a priori vertical profile at a certain altitude z , VC_i is the vertical integration
303 of the profile for the MAXDOAS cycle i and sh is the scaling height constant. We used 0.5
304 km as the scaling height constant for all the a priori profiles (Hendrick et al., 2014). Regarding
305 the VC, we assumed an AOD of 0.05 for the O₄ retrieval, while for NO₂ we applied the
306 geometrical approximation followed in Hönninger et al., 2004, taking the measured DSCD at
307 VEA 30° for every MAXDOAS cycle. This approximation assumes that most of the absorption
308 events are located below the scattering height.

309

310 With respect to the remaining atmospheric parameters, we chose typical values for
311 urban environments: surface albedo of 0.07, correlation length of 0.4 km and an a priori
312 covariance factor of 1 (see Hendrick et al., 2014). However, the most important set of
313 parameters are the atmospheric profiles such as the air number density vertical profile since it
314 is directly related to the number of O₄ absorptions, and therefore to the O₄ DSCDs. Hence the
315 relative differences, particularly for lower VEAs, between the measured and simulated O₄
316 DSCDs are usually assigned to aerosol extinction. Note however, as shown below, that
317 uncertainties in the air number density profiles - arising from uncertainties in the values or shape
318 of the temperature and pressure profiles- could also explain such differences (Fig. 4).



319

320

Figure 4. Comparison of retrieved aerosols using two different atmospheric profiles:
321 the US Standard (atmosphere A) and the US Standard adapted to the altitude above sea level
322 of Madrid (atmosphere B).

323

324

Here we compare the simulation of O₄ DSCDs using two different sets of atmospheric
325 profiles: i) the US Standard, and ii) the same profile but interpolating the pressure profile to
326 Madrid's height above sea level (mean value of 667 m). This means that the temperature profile
327 is assumed to be the same but the pressure profile is shifted less than 10%, so there are no major
328 variations within the profiles. The lower row in Fig. 4 shows that both atmospheric profiles
329 result in almost the same set of simulated O₄ DSCDs, however the aerosol extinction
330 coefficients differ significantly (although less for the surface layer coefficients), and
331 consequently, the AOD also varies. From this we infer that:

332

333

i) the retrieval is mainly driven by the measured DSCDs, which leaves a relatively
334 low weight for the chosen atmospheric profiles (pressure and temperature).
335 Therefore, we can achieve very consistent, solid correlations between the
336 measured and simulated O₄ DSCDs.

337

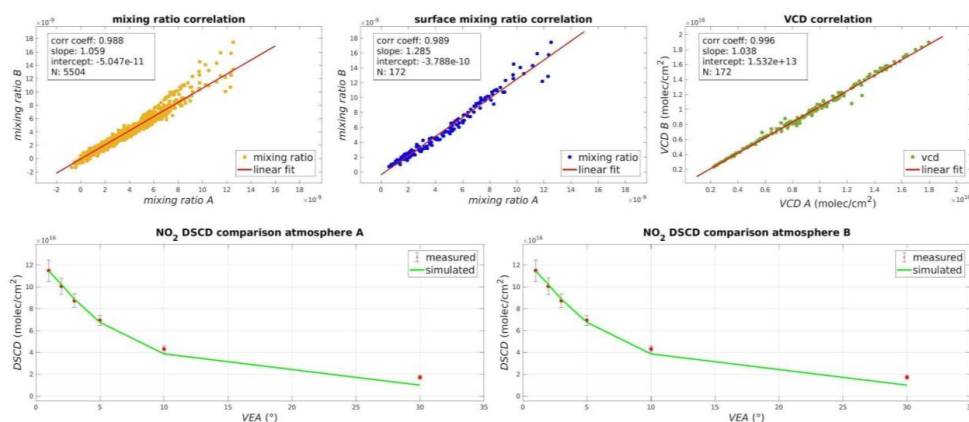
338

ii) we cannot reliably assign the extinction coefficients at each layer to particulate
339 aerosol (especially for atmospheric layers above the surface layer), but rather
340 consider them as irradiance extinction coefficients.

341



342 Furthermore, we have assessed the impact of the pressure and temperature profiles
343 choice on the trace gas retrieval. As can be noted in Fig. 5, there is no significant effect coming
344 from this choice on the simulated NO₂ DSCDs. These are basically the same (and with very
345 good agreement with the measured DSCDs), as well as the derived concentration coefficients
346 and their integration (VCD). Consequently, we have decided to use the US Standard
347 atmospheric profiles for the NO₂ retrievals in this study.
348



349
350 **Figure 5.** NO₂ retrieval comparison using two different atmospheric profiles: the US Standard
351 (atmosphere A) and the US Standard adapted to the altitude above sea level of Madrid
352 (atmosphere B).

353

354 4.3 Estimation of NO₂ horizontal gradients

355

356 Making use of the different paths that photons travel through the atmosphere for
357 different wavelengths, we can estimate the horizontal distribution of NO₂. We use the estimated
358 horizontal light paths at two wavelengths, 360.8 nm and 477 nm, for the surface layer (0-200
359 m height). The different light paths at 360.8 and 477 nm provide information about the
360 horizontal distribution of NO₂ mixing ratios within the surface layer. In order to evaluate these
361 horizontal paths, we have used our own MATLAB codes that implement the RTM equations
362 based on previous pioneering work (Solomon et al., 1987). These equations yield a vector of
363 scattering events along with their respective probabilities. If we take a VEA of 0 degrees (i.e.
364 horizontal viewing), then the scalar product of such vectors produces the length of the



365 horizontal light path. We computed this for every MAXDOAS cycle and for both wavelengths.
 366 The next step follows the “onion-peeling” approach proposed by Ortega et al. 2015 (the strong
 367 dependence of scattering with wavelength means that shorter wavelengths result in shorter light
 368 paths). Therefore, we first assign the UV (i.e. 360.8 nm) mixing ratios (mr_{uv}) and their
 369 expected horizontal paths (d_{uv}) to the first peel (mr_A , meaning zone A). Then the second peel
 370 (zone B, mr_B) can be derived as:

371

$$372 \quad mr_B = \frac{mr_{vis} \times d_{vis} - mr_{uv} \times d_{uv}}{d_{vis}} \quad (3)$$

373

374 Thus we can derive mixing ratio values (mr_a and mr_b) representative of two different
 375 horizontal distances for each VAA.

376

377 5 Results

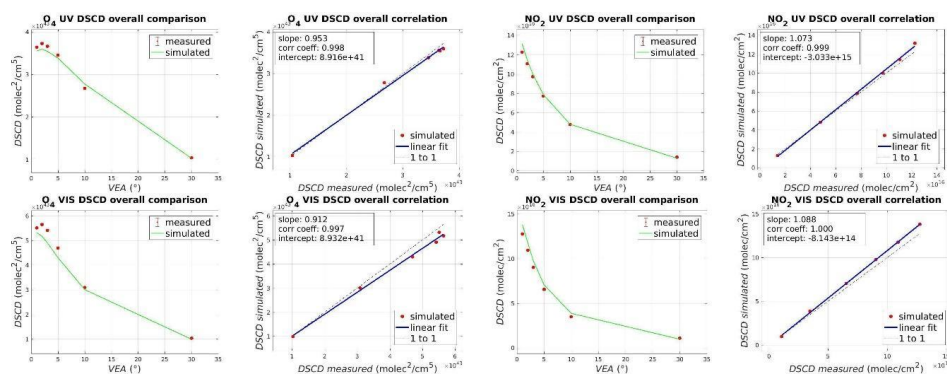
378

379 5.1 O₄ and NO₂ DSCDs assessment

380

381 Once the vertical profiles are retrieved using the RTM explained in Sect. 4, we compare
 382 the set of simulated DSCDs predicted by the model with the measured DSCDs coming from
 383 the absorption analysis. An estimation of the overall goodness of the profile retrieval comes
 384 from the correlation between the measured and simulated DSCDs for the entire campaign (Fig.
 385 6).

386



387

388 **Figure 6.** Comparison between simulated and measured DSCDs of O₄ and NO₂.

389



390 The fit between the measured and the simulated DSCDs show correlations (r^2) very
391 close to 1 for both O_4 and NO_2 in the UV and VIS regions. As mentioned before, the inverse
392 retrieval finds the optimal solution of the vertical concentration profile that generates the best
393 set of simulated DSCDs so that they match the measured ones.

394

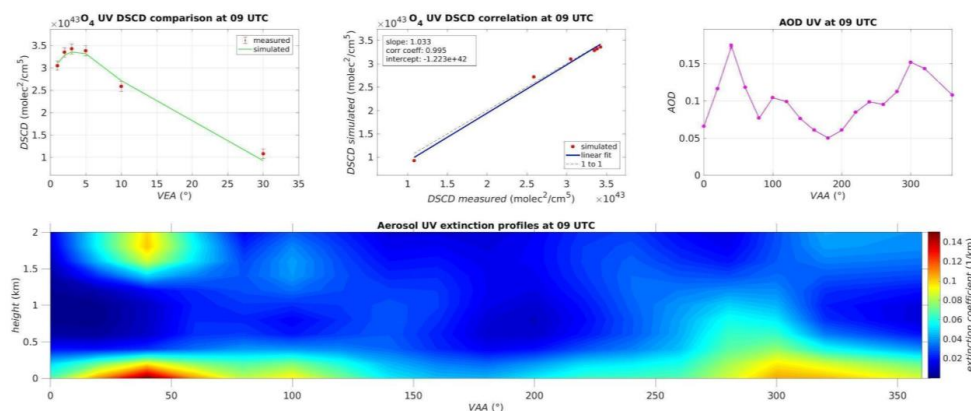
395 5.2 Two-dimensional maps

396

397 We now combine the VAA and height for each azimuthal cycle of the MAXDOAS-2D
398 to generate a two-dimensional concentration map. Fig. 7 shows an example of the O_4 retrieval
399 in the UV for a given azimuthal cycle. In addition to the profiles, Fig. 7 also shows the
400 comparison and correlation of measured and simulated DSCDs for that azimuthal cycle, along
401 with the evolution of retrieved AOD. The AOD varies between 0.05 and 0.18 within this
402 azimuthal cycle (Fig. 7, upper panel). The contour plot shows the irradiance extinction
403 coefficient profiles with maximum values of 0.14 km^{-1} (near the ground and at around 40°
404 VAA) associated with aerosol extinction (see discussion in Sect. 4.2).

405

406



407

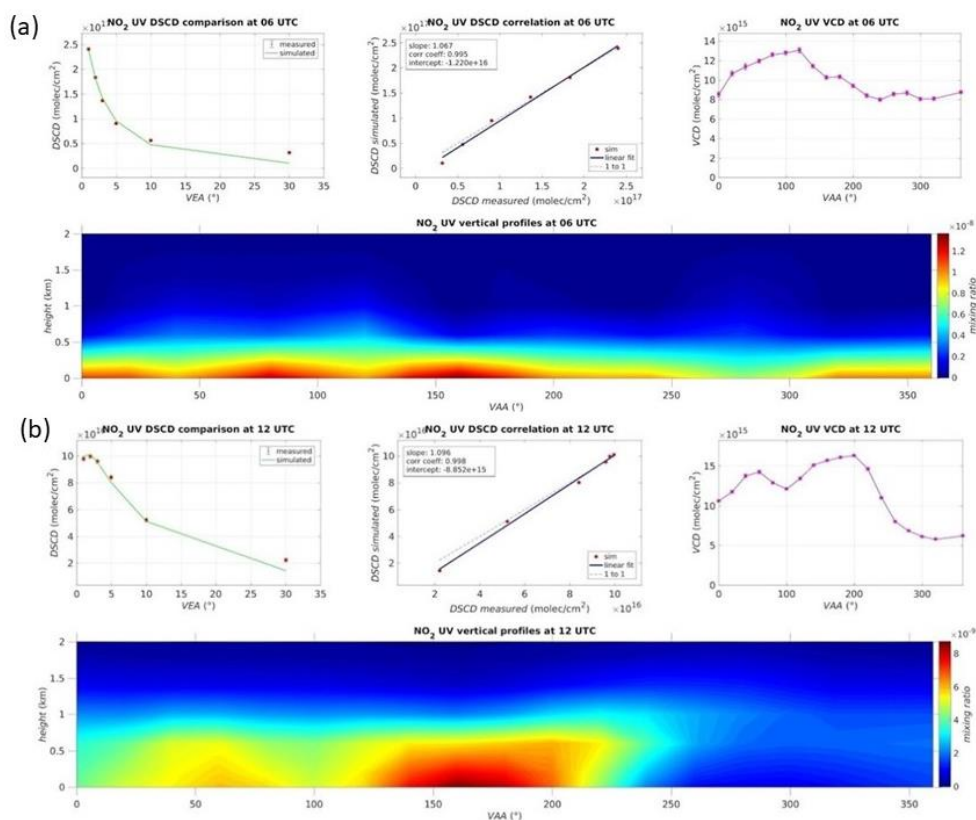
408 **Figure 7.** Example of O_4 and AOD retrievals in the UV region at 9 UTC on May 11,
409 2019. These contour plots are smoothed from adjacent VAA data points separated by 20°
410 in order to estimate the azimuthal distribution of the irradiance extinction coefficients over
411 Madrid.

412

413



414 Figure 8 presents a two-dimensional representation of NO₂ on May 11, 2019 at two
415 different hours (6 UTC and 12 UTC, respectively). Both contour plots show maximum NO₂
416 values of 12 ppbv at 6 UTC and 8 ppbv at 12 UTC, when the instrument is pointing south (i.e.
417 VAA of 180°). These values are found in the layer near the ground and are in good agreement
418 with our previous MAXDOAS observations in Madrid (Garcia-Nieto et al., 2018). The
419 retrieved azimuthal distribution of NO₂ agrees with previous reports that show higher pollution
420 levels in the southern section of Madrid (Picornell et al., 2019). NO₂ VCDs range from 5x10¹⁵
421 molecules cm⁻² (at 12 UTC and pointing at 300 ° VAA) up to 15x10¹⁵ molecules cm⁻² (at 12
422 UTC and pointing at 200° VAA), with an average value of 1x10¹⁶ molecules cm⁻². Although
423 there can be different NO_x emission rates at both times of the day (6 and 12 UTC), the increase
424 in the boundary layer height during the day could explain the similar values of VCDs at both
425 hours but generally lower surface mixing ratios at 12 UTC. Note that NO₂ is efficiently mixed
426 within the boundary layer as it develops during the day (i.e. boundary layer height usually lags
427 the solar zenith angle) (Fig. 8) (de la Paz et al., 2016).
428
429



430

431

432

433 **Figure 8.** NO_2 vertical distribution retrieved in the UV region at 6 UTC (a) and at 12 UTC (b)

434 on May 11, 2019. These contour plots are smoothed from adjacent VAA data points separated

435 by 20° in order to estimate the azimuthal distribution of NO_2 over Madrid.

436

437 5.3 Horizontal distribution of NO_2

438

439 Based on Eq. (3), we derive the horizontal distribution of NO_2 in the surface layer (0-

440 200 m height). Figure 9 shows an example of surface layer NO_2 mixing ratios over horizontal

441 distances from the MAXDOAS-2D instrument, located at the center of the plot. The highest

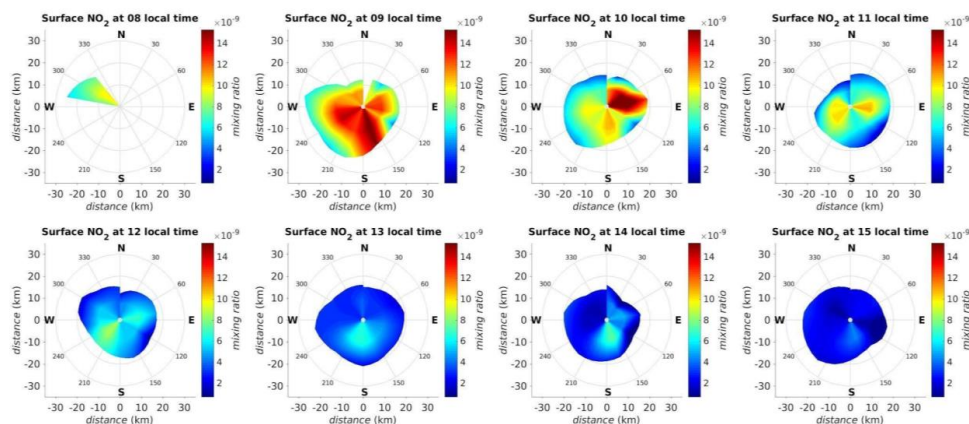
442 mixing ratios occur during the first sunlit hours (7-8 UTC), coincident with the peak in NO_x

443 emissions in Madrid (Quassdorff et al., 2016). This early morning peak is followed by a gradual



444 decrease in surface layer NO₂ mixing ratios during the day. Note that NO₂ is predominantly
445 located in the southern part of the semisphere (VAA from 90° to 270°).

446



447

448 **Figure 9.** Polar plots of NO₂ within the surface layer (0-200 m height) for May 11, 2019. Please
449 note that these contours extend over a direction perpendicular to those shown in Fig. 8. These
450 contour plots are smoothed from adjacent VAA data points separated by 20° and from the two
451 different horizontal light paths in the radial direction.

452

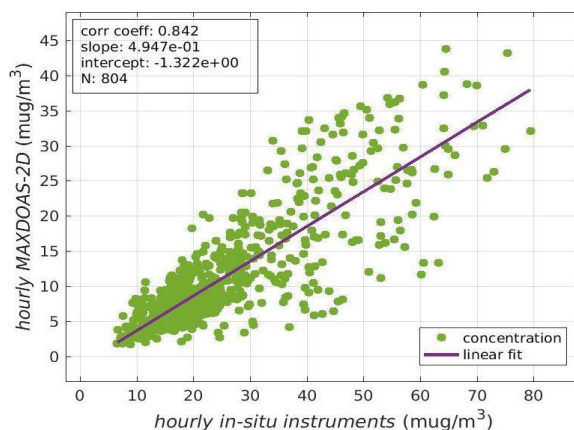
453 **5.4 Correlation with Madrid's in-situ air quality monitoring stations**

454 We suggest that MAXDOAS-2D mesoscale observations may complement the
455 information provided by the local air quality monitoring network based on reference analytical
456 techniques (according to Directive 2008/50/EC). While air quality monitors of the reference
457 network provide information about ambient concentrations in their specific locations (currently
458 24 air quality monitoring stations measure NO₂ within the city, see AM, 2019), MAXDOAS-
459 2D observations produce near ground-level concentrations averaged over the optical path in a
460 given direction. That prevents us from quantitatively comparing both types of observations.
461 Nonetheless, we analyzed their correspondence using the NO₂ concentrations measured by the
462 in-situ instruments throughout the entire city, and the NO₂ mixing ratios within the surface
463 layer derived from our MAXDOAS-2D instrument over the 2-month period (May-June, 2019).
464 For this comparison, we considered the in-situ stations that were within a distance from the
465 MAXDOAS-2D that is equal or lower than the typical horizontal light path for the UV region



466 (roughly of about 10 km). Strong gradients between the values measured by the in-situ
467 instruments are typical. Therefore, and considering that we are mainly interested in their
468 temporal correlation with respect to our MAXDOAS-2D measurements, we compare both the
469 in-situ NO₂ and surface layer MAXDOAS-2D hourly-averaged data. Note that for the
470 MAXDOAS-2D this approximately corresponds to averaging the surface layer values for each
471 azimuthal lap, given that each azimuthal lap takes approximately 1 hour to complete.

472



473

474

475 **Figure 10.** Correlation between in-situ observations from Madrid's air quality monitoring
476 network and those derived from the MAXDOAS-2D instrument for the surface layer (0-200 m
477 height).

478 Despite the different spatial representativeness, Figure 10 shows a reasonably good
479 correlation coefficient of 0.842 between both datasets for the two-month campaign. The slope
480 is lower than 1, this can be explained by the typical NO₂ vertical profiles in urban environments.
481 Simulations performed over Madrid with a high-resolution Eulerian air quality model (Borge
482 et al., 2018) yielded an exponentially decreasing with height NO₂ profile. Therefore, the
483 MAXDOAS-2D mixing ratios, which represent an average across the surface layer (0-200 m
484 height), are not expected to quantitatively match the values of in-situ instruments, located close
485 to the surface (between 0-10 m height). Nevertheless, there is a good temporal correlation
486 between in-situ and MAXDOAS-2D measurements over an extended period of time.

487

488



489 **6 Summary and Conclusions**

490

491 A complete analysis of O₄ and NO₂ vertical concentration profiles in the urban
492 atmosphere of Madrid (Spain) has been performed over two months (from May 6 to July 5,
493 2019). We analyzed the absorptions and derived the corresponding DSCDs for both trace gases
494 in the UV and VIS regions. Then, the corresponding profiles were retrieved using a RTM. In
495 this step, we assessed the impact of different atmospheric profiles (pressure and temperature)
496 in the retrieval results. The overall comparison of measured and simulated DSCDs showed that
497 they were in very good agreement in all cases, supporting the reliability of the observations.
498 This MAXDOAS-2D instrument provides a two-dimensional view (in height and VAA) of
499 concentration profiles. We have also inferred information on the horizontal gradient of NO₂
500 within the surface layer making use of the strong dependence between wavelengths and light
501 paths across the NO₂ absorption spectrum. The resulting “onion-peeling” figures indicate peak
502 values of NO₂ in the early morning and in the southern section of the city (around 180° VAA).
503 We suggest that the new mesoscale information provided by the MAXDOAS-2D instrument
504 helps in the study of pollution transport dynamics in Madrid.

505

506

507 **Author Contribution**

508

509 A.S.-L. devised the research. D.G.-N. and N.B. carried out the measurements and
510 analyzed the data. D.G.-N., N.B., R.G. and A.S.-L. analysed and interpreted the results. D.G.-N.
511 wrote the manuscript with contributions from all co-authors.

512

513 **Acknowledgements**

514

515 The authors want to thank Manuel Perez and David Armenteros for technical assistance
516 with the instrument, and David de la Paz for model assistance. This work was supported by the
517 TECNAIRE project (“Técnicas innovadoras para la evaluación y mejora de la calidad del aire
518 urbano”) S2013/MAE-2972. We would also like to thank Juan Ramón Moreta González (PI)
519 and his staff for establishing and maintaining the AERONET sites in Madrid used in this



520 investigation. We acknowledge support of the publication fee by the CSIC Open Access
521 Publication Support Initiative through its Unit of Information Resources for Research (URICI).

522

523 **References**

524

525 Benavent, N., Garcia-Nieto, D., Wang, S., & Saiz-Lopez, A.: MAX-DOAS measurements and
526 vertical profiles of glyoxal and formaldehyde in Madrid, Spain. *Atmospheric Environment*,
527 199, 357–367, 2019.

528

529 Borge, R., Santiago, J. L., de la Paz, D., Martín, F., Domingo, J., Valdés, C., Sánchez, B.,
530 Rivas, E., Rozas, M. T., Lázaro, S., Pérez, J., & Fernández, Á.: Application of a short term air
531 quality action plan in Madrid (Spain) under a high-pollution episode - Part II: Assessment from
532 multi-scale modelling. *Science of the Total Environment*, 635, 1574–1584.
533 <https://doi.org/10.1016/j.scitotenv.2018.04.323>, 2018.

534

535 Ayuntamiento de Madrid (AM): Madrid 2016 Annual Air Quality Assessment Report (Calidad
536 del aire Madrid 2019). General Directorate of Sustainability and Environmental Control,
537 Madrid City Council Available online -only Spanish version- at
538 [http://www.mambiente.munimadrid.es/opencms/export/sites/default/cal aire/Anexos/Memoria](http://www.mambiente.munimadrid.es/opencms/export/sites/default/cal aire/Anexos/Memoria s/Memoria_2019.pdf)
539 [s/Memoria_2019.pdf](http://www.mambiente.munimadrid.es/opencms/export/sites/default/cal aire/Anexos/Memoria s/Memoria_2019.pdf), 2019.

540

541 Chance, K., Kurucz, R.L.: An improved high-resolution solar reference spectrum for earth's
542 atmosphere measurements in the ultraviolet, visible, and near infrared. *J. Quant. Spectrosc.*
543 *Radiat. Transf.*; Special Issue Dedicated to Laurence S. Rothman on the Occasion of his 70th
544 Birthday 111 (9), 1289-1295, 2010.

545

546 Clémer, K., Van Roozendaal, M., Fayt, C., Hendrick, F., Hermans, C., Pinardi, G., Spurr,
547 R., Wang, P., De Mazière, M.: Multiple wavelength retrieval of tropospheric aerosol optical
548 properties from MAXDOAS measurements in Beijing. *Atmospheric Measurement Techniques*
549 3 (4), 863, 2010.

550

551 Cuevas, C., Notario, A., Adame, J. Hilboll, A., Richter, A., Burrows, J.P, Saiz-Lopez, A.:
552 Evolution of NO₂ levels in Spain from 1996 to 2012. *Sci Rep* 4, 5887, 2014.



553

554 de la Paz, D., Borge, R., & Martilli, A.: Assessment of a high resolution annual WRF-
555 BEP/CMAQ simulation for the urban area of Madrid (Spain). *Atmospheric Environment*, 144,
556 282–296. <https://doi.org/10.1016/j.atmosenv.2016.08.082>, 2016.

557

558 European Environment Agency (EEA): Air quality in Europe – 2019 report. EEA Technical
559 Report No 10/2019. ISBN: 978-92-9480-088-6. Available online at:
560 <http://www.eea.europa.eu/publications/air-quality-in-europe-2019>., 2019

561

562 Hendrick, F., Müller, J.-., Clémer, K., Wang, P., De Mazière, M., Fayt, C., Gielen, C., Hermans,
563 C., Ma, J., Pinardi, G., Stavrou, T., Vlemmix, T., Van Roozendaal, M.: Four years of ground-
564 based MAX-DOAS observations of HONO and NO₂ in the Beijing area. *Atmos. Chemical
565 Physics*, 14 (2), 765, 2014.

566

567 Garcia-Nieto, D., Benavent, N., Saiz-Lopez, A.: Measurements of atmospheric HONO vertical
568 distribution and temporal evolution in Madrid (Spain) using the MAXDOAS technique.
569 *Science of the Total Environment*. 643, 957–966, 2018.

570

571 Hönninger, G., von Friedeburg, C., Platt, U.: Multi axis differential optical absorption
572 spectroscopy (MAXDOAS). *Atmos. Chem. Phys.* 4 (1), 231-254, 2004.

573

574 Izquierdo, R., García Dos Santos, S., Borge, R., Paz, D. de la, Sarigiannis, D., Gotti, A., &
575 Boldo, E.: Health impact assessment by the implementation of Madrid City air-quality plan in
576 2020. *Environmental Research*, 183, 109021. <https://doi.org/10.1016/j.envres.2019.109021>,
577 2020.

578

579 Meller, R., Moortgat, G.K.: Temperature dependence of the absorption cross sections of
580 formaldehyde between 223 and 323 K in the wavelength range 225-375 nm. *Journal of
581 Geophysical Research: Atmosphere* 105, 7089-7101, 2009.

582

583 Monks, P. S., Granier, C., Fuzzi, S., Stohl, A., Williams, M. L., Akimoto, H., Amann,
584 M., Baklanov, A., Baltensperger, U., Bey, I., Blake, N., Blake, R. S., Carslaw, K., Cooper, O.
585 R., Dentener, F., Fowler, D., Fragkou, E., Frost, G. J., Generoso, S., ... von Glasow, R.:



- 586 Atmospheric composition change - global and regional air quality. *Atmospheric Environment*,
587 43(33), 5268–5350. <https://doi.org/10.1016/j.atmosenv.2009.08.021>, 2009
- 588
- 589 Ortega, I., Koenig, T., Sinreich, R., Thomson, D., Volkamer, R.: The CU 2-D-MAX-DOAS
590 instrument – Part 1: Retrieval of 3-D distributions of NO₂ and azimuth-dependent OVOC
591 ratios. *Atmospheric Measurement Technique*, 8, 2371-2395, 2015.
- 592
- 593 Peters, E., Wittrock, F., GroBmann, K., FrieB, U., Richter, A., Burrows, J.: Formaldehyde and
594 nitrogen dioxide over the remote western Pacific Ocean: SCIAMACHY and GOME-2
595 validation using ship-based MAX-DOAS observations. *Atmospheric Chemistry and Physics*.
596 12 (22), 11179, 2012.
- 597
- 598 Picornell, M., Ruiz, T., Borge, R. et al. Population dynamics based on mobile phone data to
599 improve air pollution exposure assessments. *J Expo Sci Environ Epidemiol* 29, 278–291.
600 <https://doi.org/10.1038/s41370-018-0058-5>, 2019.
- 601
- 602 Plane, J.M.C., Saiz-Lopez, A.: UV-Visible Differential Optical Absorption Spectroscopy
603 (DOAS). In: Heard, D.E. (Ed.), *Analytical Techniques for Atmospheric Measurement*.
604 Blackwell Publishing, Oxford, 2006.
- 605
- 606 Platt, U., Stutz, J.: *Differential Optical Absorption Spectroscopy: Principles and Applications*.
607 Springer Berlin Heidelberg, Berlin, Heidelberg, Berlin, Heidelberg, 2008.
- 608
- 609 Quaassdorff C, Borge R, Pérez J, Lumbreras J, de la Paz D, de Andrés JM. Microscale traffic
610 simulation and emission estimation in a heavily trafficked roundabout in Madrid (Spain). *Sci*
611 *Total Environ*, 566-567:416-427. doi:10.1016/j.scitotenv.2016.05.051, 2016.
- 612
- 613 Rodgers, C.D.: *Inverse Methods for Atmospheric Sounding: Theory and Practice*. World
614 Scientific Publishing, Singapore (Singapore), 2000.
- 615
- 616 Rothman, L.S., Gordon, I.E., Barber, R.J., Dothe, H., Gamache, R.R., Goldman, A., Perevalov,
617 V.L., Tashkum, S.A., Tennyson, J.: HITEMP, the high-temperature molecular spectroscopic
618 database *Journal of Quantitative Spectroscopy and Radiative Transfer*. 111 (15), 2139, 2150,
619 2010.



620

621 Saiz-Lopez, A., Borge, R., Notario, A. et al.: Unexpected increase in the oxidation capacity of
622 the urban atmosphere of Madrid, Spain. *Sci Rep* 7, 45956. <https://doi.org/10.1038/srep45956>,
623 2017.

624

625 Serdyunchenko, A., Gorshchev, V., Weber, M., Chehade, W., Burrows, J.P.: High spectral
626 resolution ozone absorption cross-sections – Part 2: temperature dependence. *Atmospheric
627 Measurement Techniques*. 7 (2), 625-636, 2014.

628

629 Solomon, S., & Sanders, Ryan W and Schmeltekopf, A. L.: On the Interpretation of Zenith Sky
630 Absorption Measurements. *Journal of Geophysical Research*, 92, 8311–8319, 1987.

631

632 Stutz, J., Kim, E.S., Platt, U., Bruno, P., Perrino, C., Febo, A.: UV-visible absorption cross
633 sections of nitrous acid. *Journal of Geophysical Research: Atmosphere*. 105, 14585-14592,
634 2000.

635

636 Thalman, R., Volkamer, R.: Temperature dependent absorption cross-sections of O₂-O₂
637 collision pairs between 340 and 630 nm and at atmospherically relevant pressure. *Physical
638 Chemistry Chemical Physics* 15 (37), 15371-15381, 2013.

639

640 Vandaele, A.C., Hermans, C., Simon, P.C., Carleer, M., Colin, R., Fally, S., Mérianne, M.F.,
641 Jenouvrier, A., Coquart, B.: Measurements of the NO₂ absorption cross-section from 42000
642 cm⁻¹ to 10000 cm⁻² (238-1000 nm) at 220 K and 294 K. *Journal of Quantitative
643 Spectroscopy and Radiative Transfer; Atmospheric Spectroscopy Application* 59 (3), 171-184
644 96, 1998.

645

646 Wagner, T., Beirle, S., Benavent, N., Bösch, T., Chan, K. L., Donner, S., Dörner, S., Fayt, C.,
647 Frieß, U., García-Nieto, D., Gielen, C., González-Bartolome, D., Gomez, L., Hendrick, F.,
648 Henzing, B., Jin, J. L., Lampel, J., Ma, J., Mies, K., Navarro, M., Peters, E., Pinardi, G.,
649 Puentedura, O., Puķīte, J., Remmers, J., Richter, A., Saiz-Lopez, A., Shaiganfar, R., Sihler, H.,
650 Van Roozendaal, M., Wang, Y., and Yela, M.: Is a scaling factor required to obtain closure
651 between measured and modelled atmospheric O₄ absorptions? An assessment of uncertainties
652 of measurements and radiative transfer simulations for 2 selected days during the MAD-CAT
653 campaign. *Atmospheric Measurement Techniques* 12, 2745–2817, 2019.



654

655 Wang, S., Cuevas, C.A., Frieß, U., Saiz-Lopez, A.: MAX-DOAS retrieval of aerosol extinction
656 properties in Madrid, Spain. *Atmospheric Measurement Techniques* 9,5089–5101, 2016.

657

658 Volkamer, R., Spietz, P., Burrows, J., Platt, U.: High-resolution absorption cross-section of
659 glyoxal in the UV-vis and IR spectral ranges. *J. Photochem. Photobiol. Chem.* 172 (1), 35-46,
660 2005.

661

662 World Health Statistics (WHO), 2019: Monitoring Health For the SDGs. World Health
663 Organization.